



HAL
open science

Normalization-Equivariant Neural Networks with Application to Image Denoising

Sébastien Herbreteau, Emmanuel Moebel, Charles Kervrann

► **To cite this version:**

Sébastien Herbreteau, Emmanuel Moebel, Charles Kervrann. Normalization-Equivariant Neural Networks with Application to Image Denoising. Conference on Neural Information Processing Systems (NeurIPS), Dec 2023, New-Orleans, United States. 10.48550/arXiv.2306.05037 . hal-04123516

HAL Id: hal-04123516

<https://hal.science/hal-04123516v1>

Submitted on 9 Jun 2023

HAL is a multi-disciplinary open access archive for the deposit and dissemination of scientific research documents, whether they are published or not. The documents may come from teaching and research institutions in France or abroad, or from public or private research centers.

L'archive ouverte pluridisciplinaire **HAL**, est destinée au dépôt et à la diffusion de documents scientifiques de niveau recherche, publiés ou non, émanant des établissements d'enseignement et de recherche français ou étrangers, des laboratoires publics ou privés.



Distributed under a Creative Commons Attribution - NonCommercial - NoDerivatives 4.0
International License

NORMALIZATION-EQUIVARIANT NEURAL NETWORKS WITH APPLICATION TO IMAGE DENOISING

Sébastien Herbreteau

Emmanuel Moebel

Charles Kervrann

Centre Inria de l'Université de Rennes, France

{sebastien.herbreteau, emmanuel.moebel, charles.kervrann}@inria.fr

ABSTRACT

In many information processing systems, it may be desirable to ensure that any change of the input, whether by shifting or scaling, results in a corresponding change in the system response. While deep neural networks are gradually replacing all traditional automatic processing methods, they surprisingly do not guarantee such normalization-equivariance (scale + shift) property, which can be detrimental in many applications. To address this issue, we propose a methodology for adapting existing neural networks so that normalization-equivariance holds by design. Our main claim is that not only ordinary convolutional layers, but also all activation functions, including the ReLU (rectified linear unit), which are applied element-wise to the pre-activated neurons, should be completely removed from neural networks and replaced by better conditioned alternatives. To this end, we introduce affine-constrained convolutions and channel-wise sort pooling layers as surrogates and show that these two architectural modifications do preserve normalization-equivariance without loss of performance. Experimental results in image denoising show that normalization-equivariant neural networks, in addition to their better conditioning, also provide much better generalization across noise levels.

1 Introduction

Sometimes wrongly confused with the invariance property which designates the characteristic of a function f not to be affected by a specific transformation \mathcal{T} applied beforehand, the equivariance property, on the other hand, means that f reacts in accordance with \mathcal{T} . Formally, invariance is $f \circ \mathcal{T} = f$ whereas equivariance reads $f \circ \mathcal{T} = \mathcal{T} \circ f$, where \circ denotes the function composition operator. Both invariance and equivariance play a crucial role in many areas of study, including physics, computer vision, signal processing and have recently been studied in various settings for deep-learning-based models [4, 5, 6, 7, 8, 9, 10, 11, 12, 13, 14].

In this paper, we focus on the equivariance of neural networks f_θ to a specific transformation \mathcal{T} , namely normalization. Although highly desirable in many applications and in spite of its omnipresence in machine learning, current neural network architectures do not equivary to normalization. With application to image denoising, for which *normalization-equivariance* is generally guaranteed for a lot of conventional methods [18, 20, 27, 22], we propose a methodology for adapting existing neural networks, and in particular denoising CNNs [30, 32, 31, 34, 33], so that *normalization-equivariance* holds by design. In short, the proposed adaptation is based on two innovations:

1. affine convolutions: the weights from one layer to each neuron from the next layer, *i.e.* the convolution kernels in a CNN, are constrained to encode affine combinations of neurons (the sum of the weights is equal to 1).
2. channel-wise sort pooling: all activation functions that apply element-wise, such as the ReLU, are substituted with higher-dimensional nonlinearities, namely two by two sorting along channels that constitutes a fast and efficient *normalization-equivariant* alternative.

Despite strong architectural constraints, we show that these simple modifications do not degrade performance and, even better, increase robustness to noise levels in image denoising both in practice and in theory.

2 Related Work

A non-exhaustive list of application fields where equivariant neural networks were studied includes graph theory, point cloud analysis and image processing. Indeed, graph neural networks are usually expected to equivary, in the sense that a permutation of the nodes of the input graph should permute the output nodes accordingly. Several specific architectures were investigated to guarantee such a property [5, 6, 7]. In parallel, rotation and translation-equivariant networks for dealing with point cloud data were proposed in a recent line of research [12, 13, 14]. A typical application is the ability for these networks to produce direction vectors consistent with the arbitrary orientation of the input point clouds, thus eliminating the need for data augmentation. Finally, in the domain of image processing, it may be desirable that neural networks produce outputs that equivary with regard to rotations of the input image, whether these outputs are vector fields [8], segmentation maps [9, 10], labels for image classification [9] or even bounding boxes for object tracking [11].

In addition to their better conditioning, equivariant neural networks by design are expected to be more robust to outliers. A spectacular example has been revealed by S. Mohan *et al.* [1] in the field of image denoising. By simply removing the additive constant (“bias”) terms in neural networks with ReLU activation functions, they showed that a much better generalization at noise levels outside the training range was ensured. Although they do not fully elucidate why biases prevent generalization, and their removal allows it, the authors establish some clues that the answer is probably linked to the *scale-equivariant* property of the resulting encoded function: rescaling the input image by a positive constant value rescales the output by the same amount.

3 Overview of normalization equivariance

3.1 Definitions and properties of three types of fundamental equivariances

We start with formal definitions of the different types of equivariances studied in this paper.

Definition 1 A function $f : \mathbb{R}^n \mapsto \mathbb{R}^m$ is said to be:

- *scale-equivariant* if $\forall x \in \mathbb{R}^n, \forall \lambda \in \mathbb{R}_*^+, f(\lambda x) = \lambda f(x)$,
- *shift-equivariant* if $\forall x \in \mathbb{R}^n, \forall \mu \in \mathbb{R}, f(x + \mu) = f(x) + \mu$,
- *normalization-equivariant* if it is both *scale-equivariant* and *shift-equivariant*:

$$\forall x \in \mathbb{R}^n, \forall \lambda \in \mathbb{R}_*^+, \forall \mu \in \mathbb{R}, f(\lambda x + \mu) = \lambda f(x) + \mu,$$

where addition with the scalar shift μ is applied element-wise.

Note that the *scale-equivariance* property is more often referred to as positive homogeneity in pure mathematics. Like linear maps that are completely determined by their values on a basis, the above described equivariant functions are actually entirely characterized by the values they take on specific subset of \mathbb{R}^n , as stated by the following proposition (see proof in Appendix D.1).

Proposition 1 (Characterizations) $f : \mathbb{R}^n \mapsto \mathbb{R}^m$ is entirely determined by its values on the:

- unit sphere \mathcal{S} of \mathbb{R}^n if it is *scale-equivariant*,
- orthogonal complement of $\text{Span}(\mathbf{1}_n)$, i.e. $\text{Span}(\mathbf{1}_n)^\perp$, if it is *shift-equivariant*,
- intersection $\mathcal{S} \cap \text{Span}(\mathbf{1}_n)^\perp$ if it is *normalization-equivariant*,

where $\mathbf{1}_n$ denotes the all-ones vector of \mathbb{R}^n .

Finally, Proposition 2 highlights three basic equivariance-preserving mathematical operations that can be used as building blocks for designing neural network architectures.

Proposition 2 (Operations preserving equivariance) Let f and g be two equivariant functions of the same type (either in *scale*, *shift* or *normalization*). Then, subject to dimensional compatibility, all of the following functions are still equivariant:

- $f \circ g$ (f composed with g),
- $x \mapsto (f(x)^\top g(x)^\top)^\top$ (concatenation of f and g),
- $(1 - t)f + tg$ for all $t \in \mathbb{R}$ (affine combination of f and g).

3.2 Examples of normalization-equivariant conventional denoisers

A (“blind”) denoiser is basically a function $f : \mathbb{R}^n \mapsto \mathbb{R}^n$ which, given a noisy image $y \in \mathbb{R}^n$, tries to map the corresponding noise-free image $x \in \mathbb{R}^n$. Since scaling up an image by a positive factor λ or adding it up a constant shift μ does not change its contents, it is natural to expect scale and shift equivariance, *i.e.* normalization equivariance, from the denoising procedure emulated by f . In image denoising, a majority of methods usually assume an additive white Gaussian noise model with variance σ^2 . The corruption model then reads $y \sim \mathcal{N}(x, \sigma^2 I_n)$, where I_n denotes the identity matrix of size n , and the noise standard deviation $\sigma > 0$ is generally passed as an additional argument to the denoiser (“non-blind” denoising). In this case, the augmented function $f : (y, \sigma) \in \mathbb{R}^n \times \mathbb{R}_*^+ \mapsto \mathbb{R}^n$ is said *normalization-equivariant* if:

$$\forall (y, \sigma) \in \mathbb{R}^n \times \mathbb{R}_*^+, \forall \lambda \in \mathbb{R}_*^+, \forall \mu \in \mathbb{R}, f(\lambda y + \mu, \lambda \sigma) = \lambda f(y, \sigma) + \mu, \quad (1)$$

as, according to the laws of statistics, $\lambda y + \mu \sim \mathcal{N}(\lambda x + \mu, (\lambda \sigma)^2 I_n)$. In what follows, we give some well-known examples of traditional denoisers that are *normalization-equivariant* (see proofs in Appendix D.2).

Noise-reduction filters: The most rudimentary methods for image denoising are the smoothing filters, among which we can mention the averaging filter or the Gaussian filter for the linear filters and the median filter which is nonlinear. These elementary “blind” denoisers all implement a *normalization-equivariant* function. More generally, one can prove that a linear filter is *normalization-equivariant* if and only if its coefficients add up to 1. In other words, *normalization-equivariant* linear filters process images by affine combinations of pixels.

Patch-based denoising: The popular N(on)-L(ocal) M(eans) algorithm [20] and its variants [22, 23, 25] consist in computing, for each pixel, an average of its neighboring noisy pixels, weighted by the degree of similarity of patches they belong to. In other words, they process images by convex combinations of pixels. More precisely, NLM can be defined as:

$$f_{\text{NLM}}(y, \sigma)_i = \frac{1}{W_i} \sum_{y_j \in \Omega(y_i)} e^{-\frac{\|p(y_i) - p(y_j)\|_2^2}{h^2}} y_j \quad \text{with} \quad W_i = \sum_{y_j \in \Omega(y_i)} e^{-\frac{\|p(y_i) - p(y_j)\|_2^2}{h^2}} \quad (2)$$

where y_i denotes the i^{th} component of vector y , $p(y_i)$ represents the vectorized patch centered at y_i , $\Omega(y_i)$ the set of its neighboring pixels and the smoothing parameter h is proportional to σ as proposed by several authors [21, 24, 25]. Defined as such, f_{NLM} is a *normalization-equivariant* function. More recently, NL-Ridge [27] and LICHl [28] propose to process images by linear combinations of similar patches and achieves state-of-the-art performance in unsupervised denoising. When restricting the coefficients of the combinations to sum to 1, that is imposing affine combination constraints, the resulting algorithms encode *normalization-equivariant* functions as well.

TV denoising: Total variation (TV) denoising [18] is finally one of the most famous image denoising algorithm, appreciated for its edge-preserving properties. In its original form [18], a TV denoiser is defined as a function $f : \mathbb{R}^n \times \mathbb{R}_*^+ \mapsto \mathbb{R}^n$ that solves the following equality-constrained problem:

$$f_{\text{TV}}(y, \sigma) = \arg \min_{x \in \mathbb{R}^n} \|x\|_{\text{TV}} \quad \text{s.t.} \quad \|y - x\|_2^2 = n\sigma^2 \quad (3)$$

where $\|x\|_{\text{TV}} := \|\nabla x\|_2$ is the total variation of $x \in \mathbb{R}^n$. Defined as such, f_{TV} is a *normalization-equivariant* function.

3.3 The case of neural networks

Deep learning hides a subtlety about normalization equivariance that deserves to be highlighted. Usually, the weights of neural networks are learned on a training set containing data all normalized to the same arbitrary interval $[a_0, b_0]$. This training procedure improves the performance and allows for more stable optimization of the model. At inference, unseen data are processed within the interval $[a_0, b_0]$ via a a - b linear normalization with $a_0 \leq a < b \leq b_0$ denoted $\mathcal{T}_{a,b}$ and defined by:

$$\mathcal{T}_{a,b} : y \mapsto (b - a) \frac{y - \min(y)}{\max(y) - \min(y)} + a. \quad (4)$$

Note that this transform is actually the unique linear one with positive slope that exactly bounds the output to $[a, b]$. The data is then passed to the trained network and its response is finally returned to the original range via the inverse operator $\mathcal{T}_{a,b}^{-1}$. This proven pipeline is actually relevant in light of the following proposition (see proof in Appendix D.1).

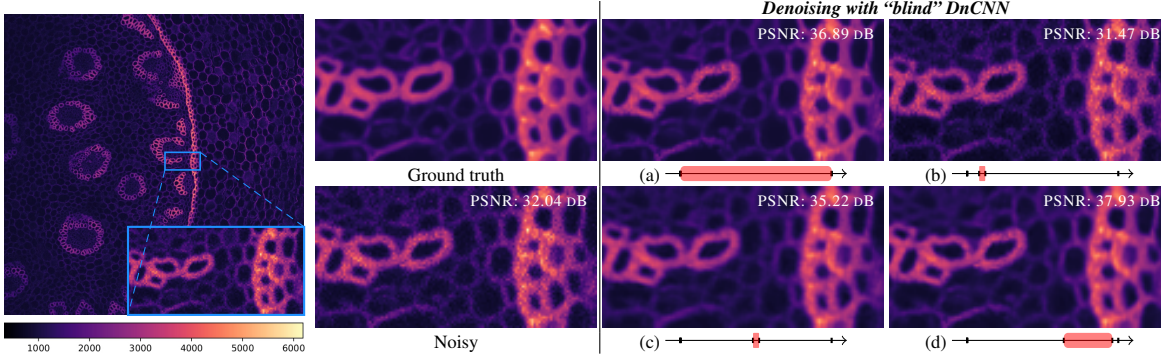


Figure 1: Influence of normalization for deep-learning-based image denoising. The raw input data is a publicly available real noisy image of the *Convallaria* dataset [17]. “Blind” DnCNN [30] with official pre-trained weights is used for denoising and is applied on four different normalization intervals displayed in red, each of which being included in $[0, 1]$ over which it was learned. PSNR is calculated with the average of 100 independent noisy static acquisitions of the same sample (called ground truth). Interestingly, the straightforward interval $[0, 1]$ does not give the best results. Normalization intervals are (a) $[0, 1]$, (b) $[0.08, 0.12]$, (c) $[0.48, 0.52]$ and (d) $[0.64, 0.96]$. In the light of the denoising results (b)-(c) and (c)-(d), DnCNN is neither *shift-equivariant*, nor *scale-equivariant*.

Table 1: Equivariance properties of several image denoisers (left: traditional, right: learning-based)

	TV	NLM	NL-Ridge	LIChi	DCT	BM3D	WNNM	DnCNN	NLRN	SwinIR	DRUNet
Scale	✓	✓	✓	✓	✓	✓	✓	✗	✗	✗	✓
Shift	✓	✓	✓	✓	✗	✗	✗	✗	✗	✗	✗

Proposition 3 $\forall a < b \in \mathbb{R}, \forall f : \mathbb{R}^n \mapsto \mathbb{R}^m, \mathcal{T}_{a,b}^{-1} \circ f \circ \mathcal{T}_{a,b}$ is a normalization-equivariant function.

While normalization-equivariance appears to be solved, a question is still remaining: how to choose the hyperparameters a and b for a given function f ? Obviously, a natural choice for neural networks is to take the same parameters a and b as in the learning phase whatever the input image is, *i.e.* $a = a_0$ and $b = b_0$, but are they really optimal? The answer to this question is generally negative. Figure 1 depicts an example of the phenomenon in image denoising, taken from a real-world application. In this example, the straightforward choice is largely sub-optimal. This suggests that there are always inherent performance leaks for deep neural networks due to the two degrees of freedom induced by the normalization (*i.e.*, choice of a and choice of b). In addition, this poor conditioning can be a source of confusion and misinterpretation in critical applications.

3.4 Categorizing image denoisers

Table 1 summarizes the equivariance properties of several popular denoisers, either conventional [18, 20, 27, 28, 19, 26, 29] or deep-learning-based [30, 32, 35, 36]. Interestingly, if *scale-equivariance* is generally guaranteed for traditional denoisers, not all of them are equivariant to shifts. In particular, the widely used algorithms DCT [19] and BM3D [26] are sensitive to offsets, mainly because the hard thresholding function at their core is not *shift-equivariant*. Regarding the deep-learning-based networks, only DRUNet [32] is insensitive to scale because it is a bias-free convolutional neural network with only ReLU activation functions [1]. In the next section, we show how to adapt existing neural architectures to guarantee *normalization-equivariance* without loss of performance and study the resulting class of parameterized functions (f_θ).

4 Design of Normalization-Equivariant Networks

4.1 Affine convolutions

To justify the introduction of a new type of convolutional layers, let us study one of the most basic neural network, namely the linear (parameterized) function $f_\theta : x \in \mathbb{R}^n \mapsto \Theta x$, where parameters Θ are a matrix of $\mathbb{R}^{m \times n}$. Indeed, f_θ can be interpreted as a dense neural network with no bias, no hidden layer and no activation function. Obviously, f_θ is always *scale-equivariant*, whatever the weights Θ . As for the *shift-equivariance*, a simple calculation shows

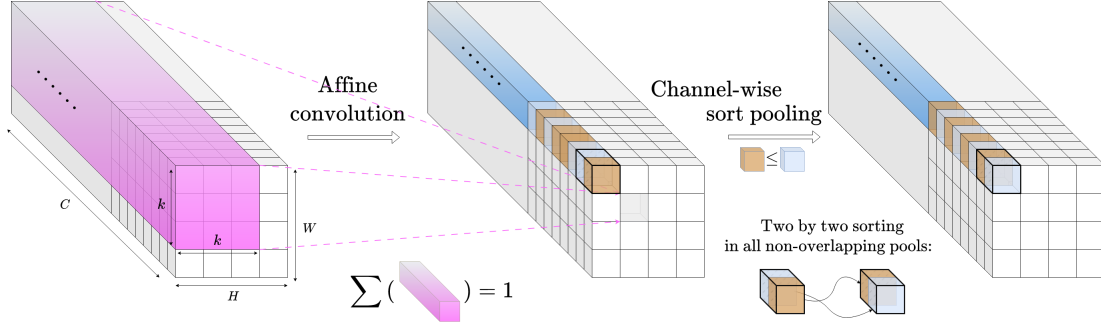


Figure 2: Illustration of the proposed alternative for replacing the traditional scheme “convolution + element-wise activation function” in convolutional neural networks: affine convolutions supersede ordinary ones by restricting the coefficients of each kernel to sum to one and the proposed sort pooling patterns introduce nonlinearities by sorting two by two the pre-activated neurons along the channels.

that:

$$x \mapsto \Theta x \text{ is shift-equivariant} \Leftrightarrow \forall x \in \mathbb{R}^n, \forall \mu \in \mathbb{R}, \Theta(x + \mu \mathbf{1}_n) = \Theta x + \mu \mathbf{1}_m \Leftrightarrow \Theta \mathbf{1}_n = \mathbf{1}_m. \quad (5)$$

Therefore, f_Θ is *normalization-equivariant* if and only if each row of matrix Θ sums to 1. In other words, for the *normalization-equivariance* to hold, the rows of Θ must encode weights of affine combinations. Transposing the demonstration to any convolutional neural network, a convolutional layer preserves the *normalization-equivariance* if and only if the weights of the each convolutional kernel sums to 1. In the following, we call such convolutional layers “affine convolutions”.

As a consequence, since *normalization-equivariance* is preserved through function composition, concatenation and affine combination (see Prop. 2), a (linear) convolutional neural network composed of only affine convolutions with no bias and possibly skip or *affine* residual connections (trainable affine combination of two layers), is guaranteed to be *normalization-equivariant*, provided that padding is performed with existing features (reflect, replicate or circular padding for example). Obviously, in their current state, these neural networks are of little interest, as linear functions do not encode best-performing functions for many applications, image denoising being no exception. Nevertheless, based on such networks, we show in the next subsection how to introduce nonlinearities without breaking the *normalization-equivariance*.

4.2 Channel-wise sort pooling as a normalization-equivariant alternative to ReLU

The first idea that comes to mind is to apply a nonlinear activation function $\varphi : \mathbb{R} \mapsto \mathbb{R}$ preserving *normalization-equivariance* after each affine convolution. In other words, we look for a nonlinear solution φ of the characteristic functional equation of *normalization-equivariant* functions (see Def. 1) for $n = 1$. Unfortunately, the unique solution is the identity function which is linear (see Prop. 1: $\mathcal{S} \cap \text{Span}(\mathbf{1}_n)^\perp = \emptyset$ for $n = 1$). Therefore, activation functions that apply element-wise are to be excluded.

To find interesting nonlinear functions, one needs to examine multi-dimensional activation functions, *i.e.* ones of the form $\varphi : \mathbb{R}^n \mapsto \mathbb{R}^m$ with $n \geq 2$. In order to preserve the dimensions of the neural layers and to limit the computational costs, we focus on the case $n = m = 2$, meaning that φ processes pre-activated neurons by pairs. According to Prop. 1, *normalization-equivariant* functions are completely determined by their values on $\mathcal{S} \cap \text{Span}(\mathbf{1}_n)^\perp$, which reduces to the characteristic set $\mathcal{C} = \{-u, u\}$, where $u = (-1/\sqrt{2}, 1/\sqrt{2})$, when considering the Euclidean distance of \mathbb{R}^2 . By arbitrarily setting $\varphi(-u) = \varphi(u) = u$, the resulting function simply reads:

$$\varphi : (x, y) \in \mathbb{R}^2 \mapsto \begin{pmatrix} \min(x, y) \\ \max(x, y) \end{pmatrix}, \quad (6)$$

which is nothing else that the sorting function in \mathbb{R}^2 . More generally, it is easy to show that all the sorting functions of \mathbb{R}^n are *normalization-equivariant*. The good news is that these functions are nonlinear as soon as $n \geq 2$. Therefore, they are candidates to replace the conventional activation functions such as the popular ReLU (rectified linear unit) function.

Since the sorting function (6) is to be applied on non-overlapping pairs of neurons, the partitioning of layers needs to be determined. In order not to mix unrelated neurons, we propose to apply this two-dimensional activation function

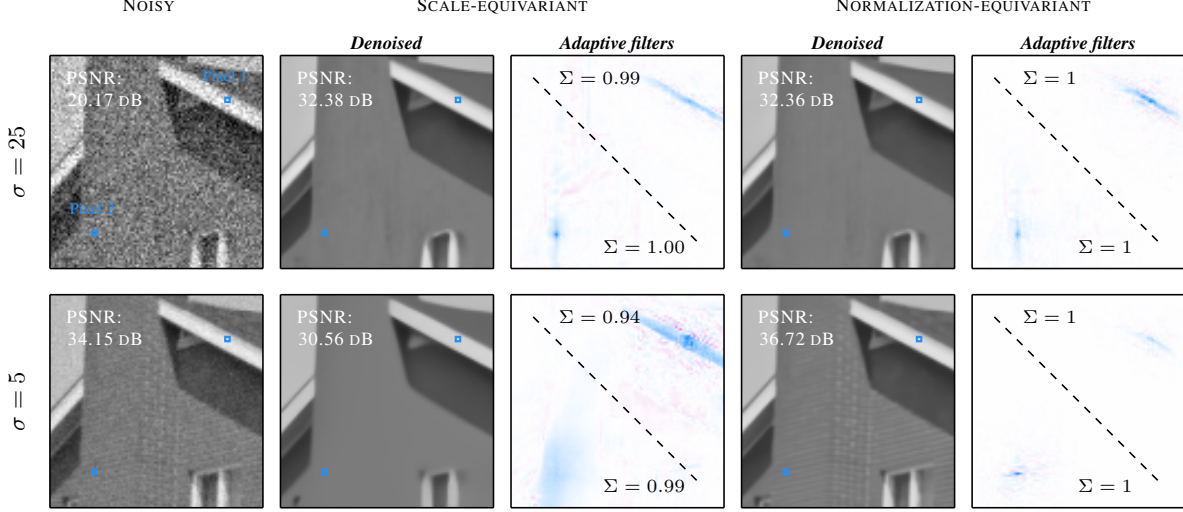


Figure 3: Visual comparisons of the generalization capabilities of a *scale-equivariant* neural network (left) and its *normalization-equivariant* counterpart (right) for Gaussian noise. Both networks were trained for Gaussian noise at noise level $\sigma = 25$ exclusively. The adaptive filters (rows of $A_\theta^{y_r}$ in Prop. 4) are indicated for two particular pixels as well as the sum of their coefficients (note that some weights are negative, indicated in red). The *scale-equivariant* network tends to excessively smooth out the image when evaluated at a lower noise level, whereas the *normalization-equivariant* network is more adaptable and considers the underlying texture to a greater extent.

channel-wisely across layers and call this operation “sort pooling” in reference to the max pooling operation, widely used for downsampling, and from which it can be effectively implemented. Figure 2 illustrates the sequence of the two proposed innovations, namely affine convolution followed by channel-wise sort pooling, to replace the traditional scheme “conv+ReLU”, while guaranteeing *normalization-equivariance*.

4.3 Encoding adaptive affine filters

Based on Prop. 2, we can formulate the following proposition which tells more about the class of parameterized functions (f_θ) encoded by the proposed networks (see proof in Appendix D.1).

Proposition 4 Let $f_\theta^{NE} : \mathbb{R}^n \mapsto \mathbb{R}^m$ be a CNN composed of only:

- affine convolution kernels with no bias and where padding is made of existing features,
- sort pooling nonlinearities,
- possibly skip or affine residual connections.

Then, f_θ^{NE} is a normalization-equivariant continuous piecewise-linear function with finitely many pieces. Moreover, on each piece represented by the vector y_r ,

$$f_\theta^{NE}(y) = A_\theta^{y_r} y, \text{ with } A_\theta^{y_r} \in \mathbb{R}^{m \times n} \text{ such that } A_\theta^{y_r} \mathbf{1}_n = \mathbf{1}_m.$$

In Prop. 4, the subscripts on $A_\theta^{y_r}$ serve as a reminder that this matrix depends on the sort pooling activation patterns, which in turn depend on both the input vector y and the weights θ . As already revealed for bias-free networks with ReLU [1], $A_\theta^{y_r}$ is the Jacobian matrix of f_θ^{NE} taken at any point y in the interior of the piece represented by vector y_r . Moreover, as $A_\theta^{y_r} \mathbf{1}_n = \mathbf{1}_m$, the output vector of such networks are locally made of fixed affine combinations of the entries of the input vector. And since a CNN has a limited receptive field centered on each pixel, f_θ^{NE} can be thought of as an adaptive filter that produces an estimate of each pixel through a custom affine combination of pixels. By examining these filters in the case of image denoising (see Fig. 3), it becomes apparent that they vary in their characteristics and are intricately linked to the contents of the underlying images. Indeed, these filters are specifically designed to cater to the specific local features of the noisy image: averaging is done over uniform areas without affecting the sharpness of edges. Note that this behavior has already been extensively studied by [1] for unconstrained filters.

The total number of fixed adaptive affine filters depends on the weights θ of the network f_θ^{NE} and is bounded by 2^S where S represents the total number of sort pooling patterns traversed to get from the receptive field to its final pixel. Obviously, this upper bound grows exponentially with S , suggesting that a limited number of sort pooling operations

may generate an extremely large number of filters. Interestingly, if ReLU activation functions were used instead, the upper bound would reach 2^{2^S} .

5 Experimental results

We demonstrate the effectiveness and versatility of the proposed methodology in the case of image denoising. To this end, we modify two well-established neural network architectures for image denoising, chosen for both their simplicity and efficiency, namely DRUNet [32]: a state-of-the-art U-Net with residual connections [2]; and FDnCNN, the unpublished flexible variant of the popular DnCNN [30]: a simple feedforward CNN that chains “conv+ReLU” layers with no downsampling, no residual connections and no batch normalization during training [3], and with a tunable noise level map as additional input [31]. We show that adapting these networks to become *normalization-equivariant* does not adversely affect performance and, better yet, increases their generalization capabilities. For each scenario, we train three variants of the original Gaussian denoising network for grayscale images: *ordinary* (original network with additive bias), *scale-equivariant* (bias-free variation with ReLU [1]) and our *normalization-equivariant* architecture (see Fig. 2). Details about training and implementations can be found in Appendix A and B; the code is available at https://github.com/sherbret/normalization_equivariant_nn/. Unless otherwise noted, all results presented in this paper are obtained with DRUNet [32]; similar outcomes can be achieved with FDnCNN [30] architecture (see Appendix C).

Finally, note that both DRUNet [32] and FDnCNN [30] can be trained as “blind” but also as “non-blind” denoisers and thus achieve increased performance, by passing an additional noisemap as input. In the case of additive white Gaussian noise of variance σ^2 , the noisemap is constant equal to $\sigma \mathbf{1}_n$ and the resulting parameterized functions can then be put mathematically under the form $f_\theta : (y, \sigma) \in \mathbb{R}^n \times \mathbb{R}_*^+ \mapsto \mathbb{R}^n$. In order to integrate this feature to *normalization-equivariant* networks as well, a slight modification of the first affine convolutional layer must be made. Indeed, by adapting the proof (5) to the case (1), we can show that the first convolutional layer must be affine with respect to the input image y only – the coefficients of the kernels acting on the image pixels add up to 1 – while the other coefficients of the kernels need not be constrained.

5.1 The proposed architectural modifications do not degrade performance

The performance, assessed in terms of PSNR values, of our *normalization-equivariant* alternative (see Fig. 2) and of its *scale-equivariant* and *ordinary* counterparts is compared in Table 2 for “non-blind” architectures on two popular datasets [37]. We can notice that the performance gap between two different variants is less than 0.05 dB at most for all noise levels, which is not significant. This result suggests that the class of parameterized functions (f_θ) currently used in image denoising can drastically be reduced at no cost. Moreover, it shows that it is possible to dispense with activation functions, such as the popular ReLU: nonlinearities can simply be brought by sort pooling patterns. In terms of subjective visual evaluation, we can draw the same conclusion since images produced by two architectural variants inside the training range are hardly distinguishable (see Fig. 3 at $\sigma = 25$).

Table 2: The PSNR (dB) results of “non-blind” deep-learning-based methods applied to popular grayscale datasets corrupted by synthetic white Gaussian noise with $\sigma = 15, 25$ and 50 .

Dataset		Set12			BSD68		
Noise level σ		15	25	50	15	25	50
DRUNet [32]	<i>ordinary</i>	33.23	30.92	27.87	31.89	29.44	26.54
	<i>scale-equiv</i>	33.25	30.94	27.90	31.91	29.48	26.59
	<i>norm-equiv</i>	33.20	30.90	27.85	31.88	29.45	26.55
FDnCNN [30]	<i>ordinary</i>	32.87	30.49	27.28	31.69	29.22	26.27
	<i>scale-equiv</i>	32.85	30.49	27.29	31.67	29.20	26.25
	<i>norm-equiv</i>	32.85	30.50	27.27	31.69	29.22	26.25

5.2 Increased robustness across noise levels

S. Mohan *et al.* [1] revealed that bias-free neural networks with ReLU, which are *scale-equivariant*, could much better generalize when evaluated at new noise levels beyond their training range, than their counterparts with bias that systematically overfit. Even if they do not fully elucidate how such networks achieve this remarkable generalization, they suggest that *scale-equivariance* certainly plays a major role. What about *normalization-equivariance* then? We

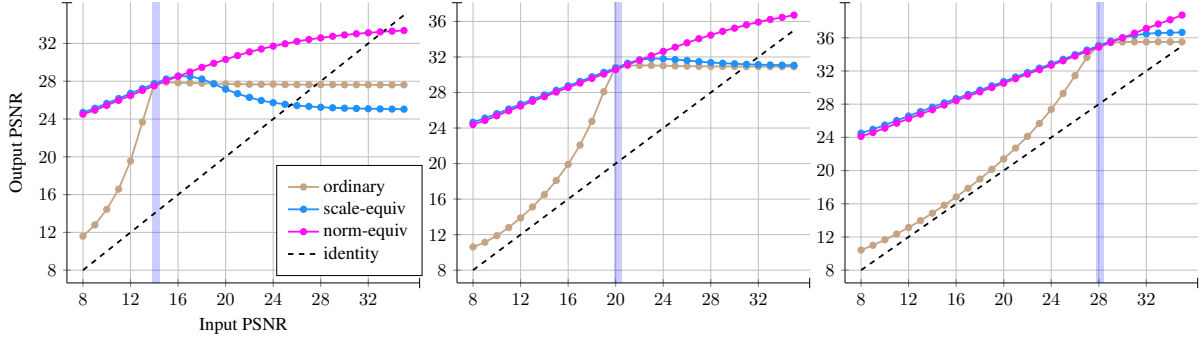


Figure 4: Comparison of the performance of our *normalization-equivariant* alternative with its *scale-equivariant* and *ordinary* counterparts for Gaussian denoising with the same architecture on Set12 dataset. The vertical blue line indicates the unique noise level on which the networks were trained exclusively (from left to right: $\sigma = 50$, $\sigma = 25$ and $\sigma = 10$). In all cases, *normalization-equivariant* networks generalize much more robustly beyond the training noise level.

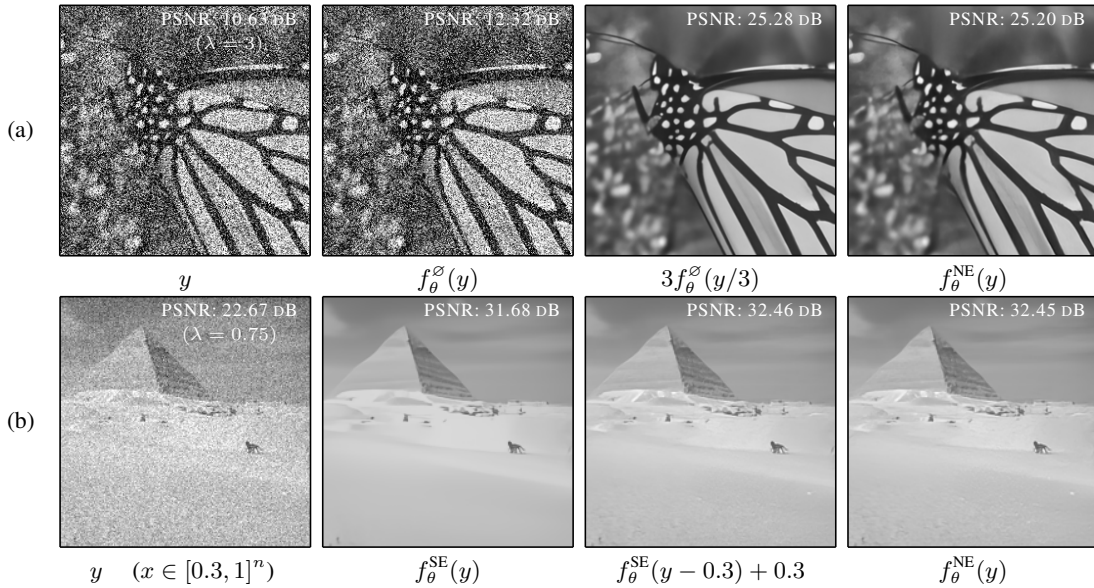


Figure 5: Denoising results for example images of the form $y = x + \lambda\varepsilon$ (see notations of subsection 5.2) with $\sigma = 25/255$ and $x \in [0, 1]^n$, by CNNs specialized for noise level σ only. f_θ^O , f_θ^{SE} and f_θ^{NE} denote the *ordinary*, *scale-equivariant* and *normalization-equivariant* variants, respectively. In order to get the best results with f_θ^O and f_θ^{SE} , it is necessary know the renormalization parameters (λ, μ) such that $(x - \mu)/\lambda$ belongs to $\mathcal{D} \subset [0, 1]^n$ (see subsection 5.2). Note that for f_θ^{SE} , it is however sufficient to know only μ as λ is implicit by construction. In contrast, f_θ^{NE} can be applied directly.

have compared the robustness faculties of the three variants of networks when trained at a fixed noise level σ for Gaussian noise. Figure 4 summarizes the explicit results obtained: *normalization-equivariance* pushes generalization capabilities of neural networks one step further. While performance is identical to their *scale-equivariant* counterparts when evaluated at higher noise levels, the *normalization-equivariant* networks are, however, much more robust at lower noise levels. This phenomenon is also illustrated in Fig. 3.

Demystifying robustness Let x be a clean patch of size n , representative of the training set on which a CNN f_θ was optimized to denoise its noisy realizations $y = x + \varepsilon$ with $\varepsilon \sim \mathcal{N}(0, \sigma^2 I_n)$ (denoising at a fixed noise level σ exclusively). Formally, we note $x \in \mathcal{D} \subset \mathbb{R}^n$, where \mathcal{D} is the space of representative clean patches of size n on which f_θ was trained. We are interested in the output of f_θ when it is evaluated at $x + \lambda\varepsilon$ (denoising at noise level $\lambda\sigma$) with $\lambda > 0$. Assuming that f_θ encodes a *normalization-equivariant* function, we have:

$$\forall \lambda \in \mathbb{R}_*^+, \forall \mu \in \mathbb{R}, f_\theta(x + \lambda\varepsilon) = \lambda f_\theta((x - \mu)/\lambda + \varepsilon) + \mu. \quad (7)$$

The above equality shows how such networks can deal with noise levels $\lambda\sigma$ different from σ : *normalization-equivariance* simply brings the problem back to the denoising of an implicitly renormalized image patch with fixed noise level σ . Note that this artificial change of noise level does not make this problem any easier to solve as the signal-to-noise ratio is preserved by normalization. Obviously, the denoising result of $x + \lambda\varepsilon$ will be all the more accurate as $(x - \mu)/\lambda$ is a representative patch of the training set. In other words, if $(x - \mu)/\lambda$ can still be considered to be in \mathcal{D} , then f_θ should output a consistent denoised image patch. For a majority of methods [30, 32, 31], training is performed within the interval $[0, 1]$ and therefore x/λ still belongs generally to \mathcal{D} for $1 < \lambda < 10$ (contraction), but this is much less true for $\lambda < 1$ (stretching) for the reason that it may exceed the bounds of the interval $[0, 1]$. This explains why *scale-equivariant* functions do not generalize well to noise levels lower than their training one. In contrast, *normalization-equivariant* functions can benefit from the implicit extra adjustment parameter μ . Indeed, there exists some cases where the stretched patch x/λ is not in \mathcal{D} but $(x - \mu)/\lambda$ is (see Fig. 5b). This is why *normalization-equivariant* networks are more able to generalize at low noise levels. Note that, based on this argument, *ordinary* neural networks trained at a fixed noise level σ can also be used to denoise images at noise level $\lambda\sigma$, provided that a correct normalization is done beforehand. However, this time the normalization is explicit: the exact scale factor λ , and possibly the shift μ , must be known (see Fig. 5a).

6 Conclusion and perspectives

In this work, we presented an original approach to adapt the architecture of existing neural networks so that they become *normalization-equivariant*, a property highly desirable and expected in many applications such that image denoising. We argue that the classical pattern “conv+ReLU” can be favorably replaced by the two proposed innovations: affine convolutions that ensure that all coefficients of the convolutional kernels sum to one; and channel-wise sort pooling nonlinearities as a substitute for all activation functions that apply element-wise, including ReLU or sigmoid functions. Despite these two important architectural changes, we show that the performance of these alternative networks is not affected in any way. On the contrary, thanks to their better-conditioning, they benefit, in the context of image denoising, from an increased interpretability and especially robustness to variable noise levels both in practice and in theory.

More generally, the proposed channel-wise sort pooling nonlinearities may potentially change the way we commonly understand neural networks: the usual paradigm that neurons are either active (“fired”) or inactive, is indeed somewhat shaken. With sort pooling nonlinearities, neurons are no longer static but they “wobble and mingle” according to the received signal. We believe that this discovery may help building new neural architectures, potentially with stronger theoretical guarantees, and more broadly, may also open the doors for novel perspectives in deep learning.

Acknowledgments

This work was supported by Bpifrance agency (funding) through the LiChIE contract. Computations were performed on the Inria Rennes computing grid facilities partly funded by France-BioImaging infrastructure (French National Research Agency - ANR-10-INBS-04-07, “Investments for the future”). We would like to thank R. Fraisse (Airbus) for fruitful discussions.

References

- [1] S. Mohan, Z. Kadkhodaie, E.P. Simoncelli and C. Fernandez-Granda, “Robust and interpretable blind image denoising via bias-free convolutional neural networks,” ICLR 2020.
- [2] K. He, X. Zhang, S. Ren, and J. Sun, “Deep residual learning for image recognition,” in *Proceedings of the IEEE conference on computer vision and pattern recognition*, pp. 770-778, 2016.
- [3] S. Ioffe and C. Szegedy, “Batch normalization: Accelerating deep network training by reducing internal covariate shift,” in *International conference on machine learning*, pmlr, pp. 448-456, 2015.
- [4] T. S. Cohen, M. Welling, “Group equivariant convolutional networks,” in *International Conference on Machine Learning*, pp. 2990–2999, 2016.
- [5] N. Keriven and G. Peyré, “Universal invariant and equivariant graph neural networks,” in *Advances in Neural Information Processing Systems*, vol. 32, 2019.
- [6] V. G. Satorras, E. Hoogeboom, and M. Welling, “E (n) equivariant graph neural networks,” in *International conference on machine learning* PMLR, pp. 9323-9332, 2021.
- [7] S. Batzner, A. Musaelian, L. Sun, *et al.*, “E (3)-equivariant graph neural networks for data-efficient and accurate interatomic potentials,” in *Nature communications*, vol. 13, no. 1, p. 2453, 2022.

- [8] D. Marcos, M. Volpi, N. Komodakis, and D. Tuia, "Rotation equivariant vector field networks," in *Proceedings of the IEEE International Conference on Computer Vision*, pp. 5048-5057, 2017.
- [9] M. Weiler, F. A. Hamprecht, and M. Storath, "Learning steerable filters for rotation equivariant cnns," in *Proceedings of the IEEE Conference on Computer Vision and Pattern Recognition*, pp. 849-858, 2018.
- [10] B. S. Veeling, J. Linmans, J. Winkens, T. Cohen, and M. Welling, "Rotation equivariant CNNs for digital pathology," in *Medical Image Computing and Computer Assisted Intervention—MICCAI: 21st International Conference, Granada, Spain, Proceedings, Part II 11*. Springer International Publishing, pp. 210-218, 2018.
- [11] D. K. Gupta, D. Arya, and E. Gavves, "Rotation equivariant siamese networks for tracking," in *Proceedings of the IEEE/CVF Conference on Computer Vision and Pattern Recognition*, pp. 12362-12371, 2021.
- [12] N. Thomas, T. Smidt, S. Kearnes, L. Yang, L. Li, K. Kohlhoff, and P. Riley, "Tensor field networks: Rotation- and translation-equivariant neural networks for 3D point clouds," *arXiv preprint arXiv:1802.08219*, 2018.
- [13] F. Fuchs, D. Worrall, V. Fischer, and M. Welling, (2020). "Se (3)-transformers: 3d roto-translation equivariant attention networks," in *Advances in Neural Information Processing Systems*, vol. 33, pp. 1970-1981, 2020.
- [14] G. Bökman, F. Kahl, and A. Flinth, "Zz-net: A universal rotation equivariant architecture for 2d point clouds," in *Proceedings of the IEEE/CVF Conference on Computer Vision and Pattern Recognition*, pp. 10976-10985, 2022.
- [15] K. Fukushima, Neocognitron: "A self-organizing neural network model for a mechanism of pattern recognition unaffected by shift in position," in *Biol. Cybernetics*, vol.36, pp. 193–202, 1980.
- [16] Y. LeCun, B. Boser, J. S. Denker, D. Henderson, R. E. Howard, W. Hubbard, and L. D. Jackel, "Backpropagation applied to handwritten zip code recognition," in *Neural Computation*, vol. 1, no. 4, pp. 541–551, 1989.
- [17] M. Prakash, M. Lalit, P. Tomancak, A. Krul, and F. Jug, "Fully unsupervised probabilistic noise2void" in *IEEE 17th International Symposium on Biomedical Imaging (ISBI)*, pp. 154-158, 2020.
- [18] L. I. Rudin, S. Osher, and E. Fatemi, "Nonlinear total variation based noise removal algorithms," in *Physica D: nonlinear phenomena*, vol. 60, pp. 259-268, 1992.
- [19] G. Yu and G. Sapiro, "DCT image denoising: a simple and effective image denoising algorithm," in *Image Processing On Line*, vol. 1, pp. 292–296, 2011.
- [20] A. Buades, B. Coll, and J.-M. Morel, "A review of image denoising algorithms, with a new one," in *SIAM Journal on Multiscale Modeling and Simulation*, vol. 4, no. 2, pp. 490-530, 2005.
- [21] A. Buades, B. Coll, and J.-M. Morel, "A non-local algorithm for image denoising," in *Proc. IEEE Comput. Soc. Conf. Comput. Vis. Pattern Recognit.*, San Diego, CA, USA, pp. 60–65, 2005.
- [22] Q. Jin, I. Grama, C. Kervrann, and Q. Liu, "Non-local means and optimal weights for noise removal," in *SIAM Journal on Imaging Sciences*, vol. 10, no. 4, pp. 1878-1920, 2017.
- [23] C. Louchet and L. Moisan, "Total variation as a local filter," *SIAM Journal on Imaging Sciences*, vol. 4, no. 2, pp. 651-694, 2011.
- [24] J. V. Manjon, J. C. Caballero, J. J. Lull, G. G. Martí, L. M. Bonmati, and M. Robles, "MRI denoising using non local means," in *Med. Image. Anal.*, vol. 12, no. 4, pp. 514-523, 2008.
- [25] V. Duval, J. F. Aujol, and Y. Gousseau, "On the parameter choice for the non-local means," Tech. Rep. HAL-00468856, 2010.
- [26] K. Dabov, A. Foi, V. Katkovnik, and K. Egiazarian, "Image denoising by sparse 3D transform-domain collaborative filtering," in *IEEE Transactions on Image Processing*, vol. 16, no. 8, pp. 2080–2095, 2007.
- [27] S. Herbreteau and C. Kervrann, "Towards a Unified View of Unsupervised Non-Local Methods for Image Denoising: The NL-Ridge Approach," in *2022 IEEE International Conference on Image Processing (ICIP)*, pp. 3376-3380, Bordeaux, France, 2022.
- [28] S. Herbreteau and C. Kervrann, "Unsupervised Linear and Iterative Combinations of Patches for Image Denoising", arXiv preprint arXiv:2212.00422, 2022.
- [29] S. Gu, L. Zhang, W. Zuo, and X. Feng, "Weighted Nuclear Norm Minimization with Application to Image Denoising," in *IEEE Conference on Computer Vision and Pattern Recognition*, Columbus, OH, USA, 2014, pp. 2862-2869.
- [30] K. Zhang, W. Zuo, Y. Chen, D. Meng, and L. Zhang, "Beyond a gaussian denoiser: residual learning of deep CNN for image denoising," in *IEEE Transactions on Image Processing*, vol. 26, no. 7, pp. 3142–3155, 2017.
- [31] K. Zhang, W. Zuo, and L. Zhang, "FFDNet: Toward a Fast and Flexible Solution for CNN based Image Denoising," in *IEEE Transactions on Image Processing*, vol. 27, no. 9, pp. 4608–4622, 2018.
- [32] K. Zhang, Y. Li, W. Zuo, L. Zhang, L. Van Gool, and R. Timofte, "Plug-and-play image restoration with deep denoiser prior," in *IEEE Transactions on Pattern Analysis and Machine Intelligence*, 2021.
- [33] X. Mao, C. Shen, and Y. Yang. "Image restoration using very deep convolutional encoder-decoder networks with symmetric skip connections," in *Advances in Neural Information Processing Systems*, pp. 2802–2810, 2016.
- [34] Y. Chen and T. Pock, "Trainable nonlinear reaction diffusion: A flexible framework for fast and effective image restoration," in *IEEE Transactions on Pattern Analysis and Machine Intelligence*, vol. 39, no. 6, pp. 1256–1272, 2017.

- [35] Ding Liu, Bihan Wen, Yuchen Fan, Chen Change Loy, and Thomas S Huang, “Non-local recurrent network for image restoration,” in *Advances in Neural Information Processing Systems*, pp. 1673–1682, 2018.
- [36] J. Liang, J. Cao, G. Sun, K. Zhang, L. Van Gool, and R. Timofte, “Swinir: Image restoration using swin transformer,” in *IEEE International Conference on Computer Vision Workshops*, pp. 1833–1844, 2021.
- [37] D. Martin, C. Fowlkes, D. Tal, and J. Malik, “A database of human segmented natural images and its application to evaluating segmentation algorithms and measuring ecological statistics,” in *International Conference on Computer Vision*, vol. 2, pp. 416–423, 2001.
- [38] D. Martin, C. Fowlkes, D. Tal, and J. Malik, “A database of human segmented natural images and its application to evaluating segmentation algorithms and measuring ecological statistics,” in *International Conference on Computer Vision*, vol. 2, pp. 416–423, 2001.
- [39] K. Ma, Z. Duanmu, Q. Wu, Z. Wang, H. Yong, H. Li, and L. Zhang, “Waterloo exploration database: New challenges for image quality assessment models,” in *IEEE Transactions on Image Processing*, vol. 26, no. 2, pp. 1004–1016, 2017.
- [40] E. Agustsson and R. Timofte, “Ntire 2017 challenge on single image super-resolution: Dataset and study,” in *IEEE Conference on Computer Vision and Pattern Recognition (CVPR) Workshops*, Jul. 2017.
- [41] B. Lim, S. Son, H. Kim, S. Nah, and K. M. Lee, “Enhanced deep residual networks for single image super-resolution,” in *2017 IEEE Conference on Computer Vision and Pattern Recognition Workshops (CVPRW)*, 2017, pp. 1132–1140.
- [42] D. Kingma and J. Ba, “Adam: A method for stochastic optimization,” in *International Conference for Learning Representations*, 2015.
- [43] W. Shi, J. Caballero, F. Huszár, J. Totz, A. P. Aitken, R. Bishop, D. Rueckert and Z. Wang, “Real-time single image and video super-resolution using an efficient sub-pixel convolutional neural network,” in *Proceedings of the IEEE conference on computer vision and pattern recognition*, pp. 1874–1883, 2016.

A Description of the denoising architectures and implementation

A.1 Description of models

DRUNet: DRUNet [32] is a U-Net architecture, and as such has an encoder-decoder type pathway, with residual connections [2]. Spatial downsampling is performed using 2×2 convolutions with stride 2, while spatial upsampling leverages 2×2 transposed convolutions with stride 2 (which is equivalent to a 1×1 sub-pixel convolution [43]). The number of channels in each layer from the first scale to the fourth scale are 64, 128, 256 and 512, respectively. Each scale is composed of 4 successive residual blocks “ 3×3 conv + ReLU + 3×3 conv”.

FDnCNN: FDnCNN [30] is the unpublished flexible variant of the popular DnCNN [30]. It consists of 20 successive 3×3 convolutional layers with 64 channels each and ReLU nonlinearities. As opposed to DnCNN, FDnCNN does not use neither batch normalization [3] for training, nor residual connections [2] and can handle an optional noisemap (concatenated with the input noisy image). Note that this architecture does not use downsampling or upsampling. Finally, the authors [30] recommend to train it by minimizing the ℓ_1 loss instead of the mean squared error (MSE).

A.2 Description of variants

Ordinary: The *ordinary* variant is built by appending additive constant (“bias”) terms after each convolution of the original architecture. Note that the original FDnCNN [30] model is already in the *ordinary* mode.

Scale-equivariant: Since both models (DRUNet and FDnCNN) use only ReLU activation functions, removing all additive constant (“bias”) terms is sufficient to ensure *scale-equivariance* [1]. Note that the original DRUNet [32] model is already in the *scale-equivariant* mode.

Normalization-equivariant: All convolutions are replaced by the proposed affine-constrained convolutions without “bias” and with reflect padding, and the proposed channel-wise sort pooling patterns supersede ReLU nonlinearities. Moreover, classical residual connections are replaced by *affine* residual connections (the sum of two layers l_1 and l_2 is replaced by their affine combination $(1 - t)l_1 + tl_2$ where t is a trainable scalar parameter).

A.3 Practical implementation of normalization-equivariant networks

The channel-wise sort pooling operations can be efficiently implemented by concatenating the sub-layer obtained with channel-wise one-dimensional max pooling with kernel size 2 and its counterpart obtained with min pooling. Note that intertwining these two sub-layers to comply with the original definition is not necessary in practice (although performed anyway in our implementation), since the order of the channels in a CNN is arbitrary.

Regarding the implementation of affine convolutions for training, each unconstrained kernel can be in practice “telescoped” with its circular shifted version (this way, the sum of the resulting trainable coefficients cancels out) and then the inverse of the kernel size is added element-wise as a non-trainable offset. Despite this over-parameterized form (involving an extra degree of freedom), we found this solution to be more easy to use in practice. Moreover, it ensures that all coefficients of the affine kernels follow the same law at initialization. Another possibility is to set an arbitrary coefficient of the kernel (the last one for instance) equal to one minus the sum of all the other coefficients. Note that the solution consisting in dividing each kernel coefficient by the sum of all the other coefficients does not work because it generates numerical instabilities as the divisor may zero, or close to zero.

All our implementations are written in Python and are based on the PyTorch library. The code is available at https://github.com/sherbret/normalization_equivariant_nn/.

B Description of datasets and training details

We use the same large training set as in [32] for all the models and all the experiments, composed of 8,694 images, including 400 images from the Berkeley Segmentation Dataset BSD400 [38], 4,744 images from the Waterloo Exploration Database [39], 900 images from the DIV2K dataset [40], and 2,750 images from the Flickr2K dataset [41]. This training set is augmented via random vertical and horizontal flips and random 90° rotations. The dataset BSD32 [38], composed of the 32 images, is used as validation set to control training and select the best model at the end. Finally, the two datasets Set12 and BSD68 [38], strictly disjoint from the training and validation sets, are used for testing.

All the models f_θ are optimized by minimizing the average reconstruction error between the denoised images $\hat{x} = f_\theta(x + \varepsilon)$, where $\varepsilon \sim \mathcal{N}(0, \sigma^2 I_n)$, and ground-truths x with Adam algorithm [42]. For “non-blind” models, the noise level σ is randomly chosen from [1, 50] during training. The training parameters, specific to each model and its variants, are guided by the instructions of the original papers [32, 30], to the extent possible, and are summarized in Table 3. Note that each training iteration consists in a gradient pass on a batch composed of patches randomly cropped from training images. *Normalization-equivariant* variants need a longer training and always use a constant learning rate (speed improvements are however certainly possible by adapting the learning rate throughout optimization, but we did not investigated much about it). Furthermore, contrary to [32] where the ℓ_1 loss function is recommended to achieve better performance, supposedly due to its outlier robustness properties, we obtained slightly better results with the usual mean squared error (MSE) loss when dealing with *normalization-equivariant* networks. Training was performed with a Quadro RTX 6000 GPU.

Table 3: Training parameters. * indicates that it is divided by half every 100,000 iterations.

Model	Batch size	Patch size	Loss function	Learning rate	Number of iterations	
DRUNet [32]	<i>ordinary</i>	16	128×128	ℓ_1	$1e-4^*$	800,000
	<i>scale-equiv</i>	16	128×128	ℓ_1	$1e-4^*$	800,000
	<i>norm-equiv</i>	16	128×128	MSE	$1e-4$	1,800,000
FDnCNN [30]	<i>ordinary</i>	128	70×70	ℓ_1	$1e-4$	500,000
	<i>scale-equiv</i>	128	70×70	ℓ_1	$1e-4$	500,000
	<i>norm-equiv</i>	128	70×70	MSE	$1e-4$	900,000

C Additional results

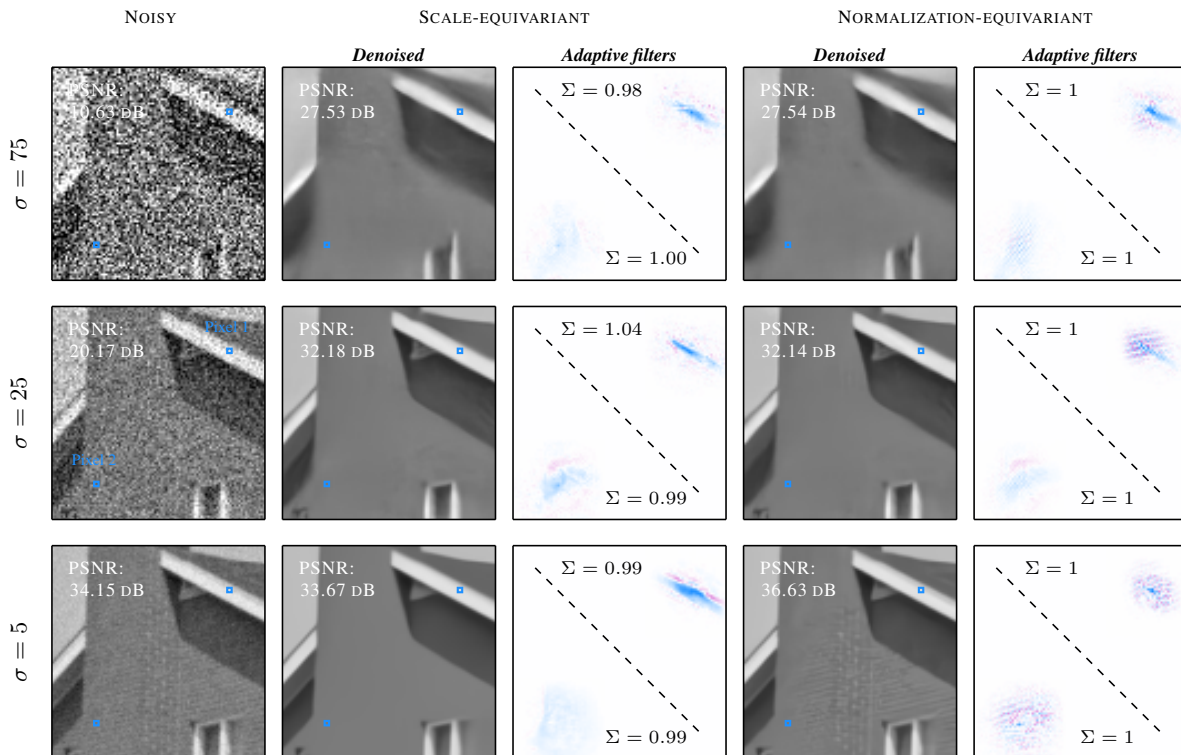


Figure 6: Visual comparisons of the generalization capabilities of a *scale-equivariant* FDnCNN [30] (left) and its *normalization-equivariant* counterpart (right) for Gaussian noise. Both networks were trained for Gaussian noise at noise level $\sigma = 25$ exclusively. The adaptive filters (rows of $A_\theta^{y_r}$ in Prop. 4) are indicated for two particular pixels as well as the sum of their coefficients (note that some weights are negative, indicated in red). The *scale-equivariant* network tends to excessively smooth out the image when evaluated at a lower noise level, whereas the *normalization-equivariant* network is more adaptable and considers the underlying texture to a greater extent.

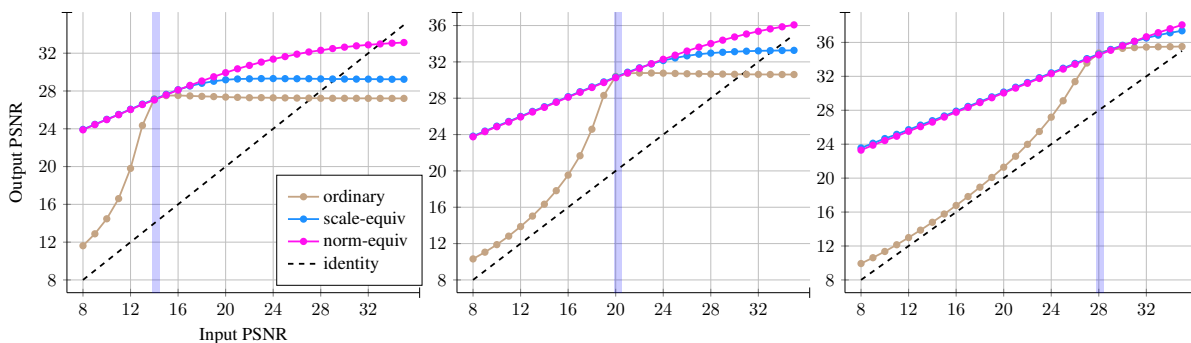


Figure 7: Comparison of the performance of our *normalization-equivariant* FDnCNN [30] with its *scale-equivariant* and *ordinary* counterparts for Gaussian denoising on the Set12 dataset. The vertical blue line indicates the unique noise level on which the networks were trained exclusively (from left to right: $\sigma = 50$, $\sigma = 25$ and $\sigma = 10$). In all cases, *normalization-equivariant* networks generalize much more robustly beyond the training noise level.

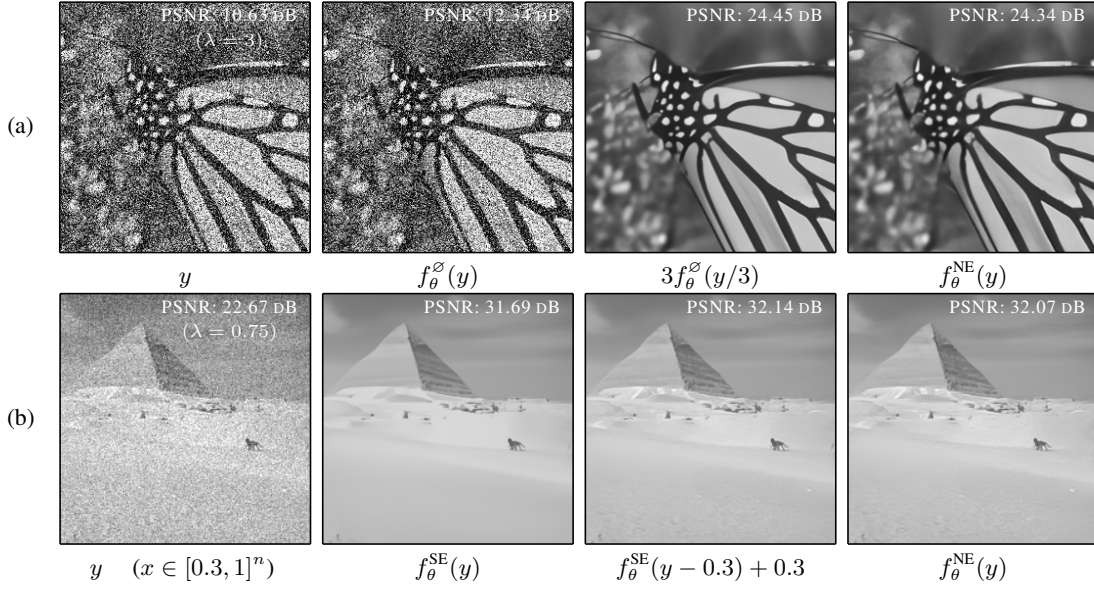


Figure 8: Denoising results for example images of the form $y = x + \lambda\varepsilon$ with $\sigma = 25/255$ and $x \in [0, 1]^n$, by FDnCNN [30] specialized for noise level σ only. Here, f_θ^O , f_θ^{SE} and f_θ^{NE} denote the *ordinary*, *scale-equivariant* and *normalization-equivariant* variants, respectively.

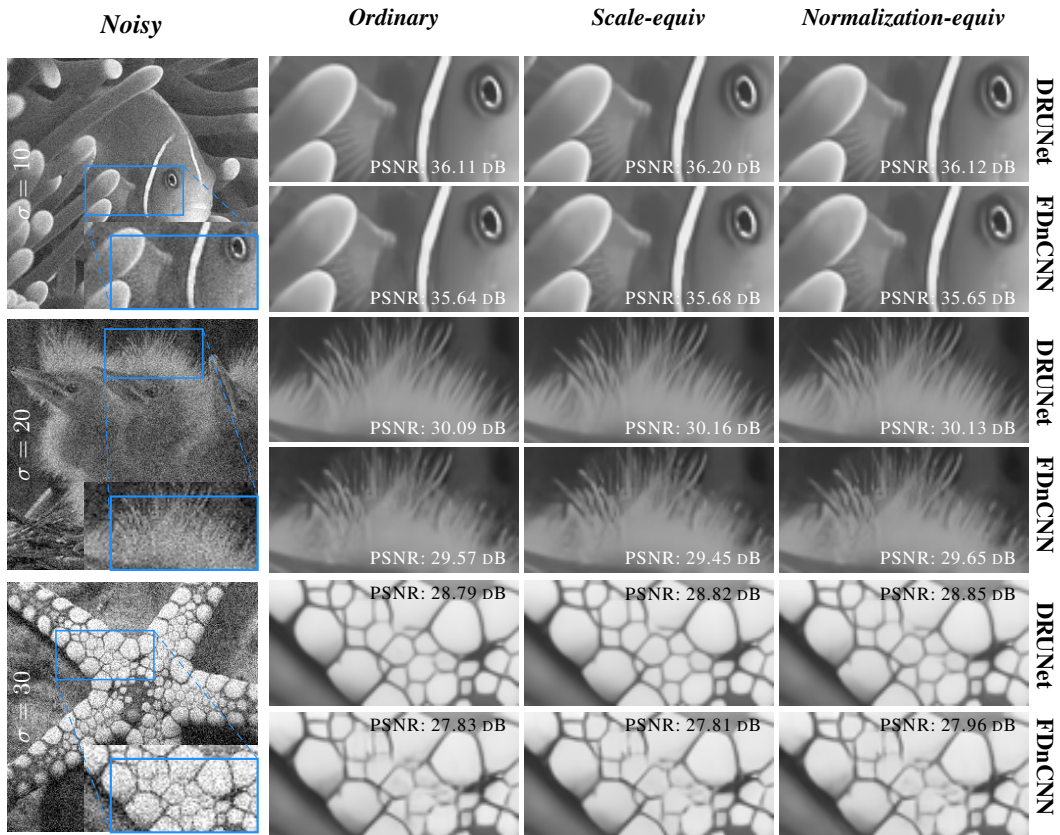


Figure 9: Qualitative comparison of image denoising results with synthetic white Gaussian noise for “non-blind” models. Regardless of the variant of a model, the denoising results are visually similar.

D Mathematical proofs

D.1 Proofs of Propositions

Proposition 1 (Characterizations)

Proof: For each type of equivariance, both existence and uniqueness of f must be proven. Let $\mathbf{0}_n$ be the zero vector of \mathbb{R}^n and $(y_x)_{x \in \mathcal{C}}$ the values that f takes on its characteristic set \mathcal{C} .

Scale-equivariance:

- Uniqueness: Let f and g two *scale-equivariant* functions such that $\forall x \in \mathcal{S}, f(x) = g(x)$. First of all, for any *scale-equivariant* function $h, h(\mathbf{0}_n) = h(2 \cdot \mathbf{0}_n) = 2h(\mathbf{0}_n)$, hence $h(\mathbf{0}_n) = \mathbf{0}_m$. Therefore, $f(\mathbf{0}_n) = g(\mathbf{0}_n) = \mathbf{0}_m$.

Let $x \in \mathbb{R}^n \setminus \{\mathbf{0}_n\}$. As $\frac{x}{\|x\|} \in \mathcal{S}$, we have $f(\frac{x}{\|x\|}) = g(\frac{x}{\|x\|}) \Rightarrow \frac{1}{\|x\|}f(x) = \frac{1}{\|x\|}g(x) \Rightarrow f(x) = g(x)$. Finally, $f = g$.

- Existence: Let $f : x \in \mathbb{R}^n \mapsto \begin{cases} \|x\| \cdot y_{\frac{x}{\|x\|}} & \text{if } x \neq \mathbf{0}_n \\ \mathbf{0}_m & \text{otherwise} \end{cases}$. Note that $\forall x \in \mathcal{S}, f(x) = y_x$. Let $x \in \mathbb{R}^n$ and $\lambda \in \mathbb{R}_*^+$. If $x \neq \mathbf{0}_n$, $f(\lambda x) = \|\lambda x\| \cdot y_{\frac{\lambda x}{\|\lambda x\|}} = \lambda \|x\| \cdot y_{\frac{x}{\|x\|}} = \lambda f(x)$ and if $x = \mathbf{0}_n$ $f(\lambda x) = \mathbf{0}_m = \lambda f(x)$, hence f is *scale-equivariant*.

Shift-equivariance:

- Uniqueness: Let f and g two *shift-equivariant* functions such that $\forall x \in \text{Span}(\mathbf{1}_n)^\perp, f(x) = g(x)$. Let $x \in \mathbb{R}^n$. By orthogonal decomposition of \mathbb{R}^n into $\text{Span}(\mathbf{1}_n)^\perp$ and $\text{Span}(\mathbf{1}_n)$:

$$\exists! (x_1, x_2) \in \text{Span}(\mathbf{1}_n)^\perp \times \text{Span}(\mathbf{1}_n), x = x_1 + x_2.$$

Then, $f(x) = f(x_1 + x_2) = f(x_1) + x_2 = g(x_1) + x_2 = g(x_1 + x_2) = g(x)$.

- Existence: Let $f : x \in \mathbb{R}^n \mapsto y_{x_1} + x_2$, where $x = x_1 + x_2$ is the unique decomposition such that $x_1 \in \text{Span}(\mathbf{1}_n)^\perp$ and $x_2 \in \text{Span}(\mathbf{1}_n)$. Note that $\forall x \in \text{Span}(\mathbf{1}_n)^\perp, f(x) = y_x$. Let $x \in \mathbb{R}^n$ and $\mu \in \mathbb{R}$. $f(x + \mu) = y_{x_1} + x_2 + \mu \mathbf{1}_m = f(x) + \mu$ as if x orthogonally decomposes into $x_1 + x_2$ with $x_1 \in \text{Span}(\mathbf{1}_n)^\perp$ and $x_2 \in \text{Span}(\mathbf{1}_n)$, then $x + \mu$ orthogonally decomposes into $x_1 + (x_2 + \mu \mathbf{1}_m)$. f is then *shift-equivariant*.

Normalization-equivariance:

- Uniqueness: Let f and g two *normalization-equivariant* functions such that $\forall x \in \mathcal{S} \cap \text{Span}(\mathbf{1}_n)^\perp, f(x) = g(x)$. First, as f and g are *a fortiori scale-equivariant*, $f(\mathbf{0}_n) = g(\mathbf{0}_n) = \mathbf{0}_m$. Let $x \in \mathbb{R}^n \setminus \{\mathbf{0}_n\}$. By orthogonal decomposition of \mathbb{R}^n into $\text{Span}(\mathbf{1}_n)^\perp$ and $\text{Span}(\mathbf{1}_n)$:

$$\exists! (x_1, x_2) \in \text{Span}(\mathbf{1}_n)^\perp \times \text{Span}(\mathbf{1}_n), x = x_1 + x_2.$$

If $x_1 = \mathbf{0}_n$, $f(x) = f(\mathbf{0}_n + x_2) = f(\mathbf{0}_n) + x_2 = \mathbf{0}_m + x_2 = x_2$. Likewise, $g(x) = x_2$, hence $f(x) = g(x)$. Else, if $x_1 \neq \mathbf{0}_n$, $f(x) = f(x_1 + x_2) = f(x_1) + x_2 = \|x_1\|f(\frac{x_1}{\|x_1\|}) + x_2 = \|x_1\|g(\frac{x_1}{\|x_1\|}) + x_2 = g(x_1) + x_2 = g(x_1 + x_2) = g(x)$, as $\frac{x_1}{\|x_1\|} \in \mathcal{S} \cap \text{Span}(\mathbf{1}_n)^\perp$. Finally, $f = g$.

- Existence: Let $f : x \in \mathbb{R}^n \mapsto \begin{cases} \|x_1\| \cdot y_{\frac{x_1}{\|x_1\|}} + x_2 & \text{if } x_1 \neq \mathbf{0}_n \\ x_2 & \text{otherwise} \end{cases}$, where $x = x_1 + x_2$ is the unique decomposition such that $x_1 \in \text{Span}(\mathbf{1}_n)^\perp$ and $x_2 \in \text{Span}(\mathbf{1}_n)$. Note that $\forall x \in \mathcal{S} \cap \text{Span}(\mathbf{1}_n)^\perp, f(x) = y_x$. Let $x \in \mathbb{R}^n$, $\lambda \in \mathbb{R}_*^+$ and $\mu \in \mathbb{R}$. x decomposes orthogonally into $x_1 + x_2$ with $x_1 \in \text{Span}(\mathbf{1}_n)^\perp$ and $x_2 \in \text{Span}(\mathbf{1}_n)$, and we have $f(\lambda x + \mu) = f(\lambda x_1 + (\lambda x_2 + \mu))$, where $\lambda x_1 + (\lambda x_2 + \mu)$ is the orthogonal decomposition of $\lambda x + \mu$ into $\text{Span}(\mathbf{1}_n)^\perp$ and $\text{Span}(\mathbf{1}_n)$.

If $x_1 = \mathbf{0}_n$, then $\lambda x_1 = \mathbf{0}_n$ and $f(\lambda x + \mu) = \lambda x_2 + \mu = \lambda f(x) + \mu$.

Else, if $x_1 \neq \mathbf{0}_n$, then $\lambda x_1 \neq \mathbf{0}_n$, and $f(\lambda x + \mu) = \|\lambda x_1\| \cdot y_{\frac{\lambda x_1}{\|\lambda x_1\|}} + (\lambda x_2 + \mu) = \lambda (\|x_1\| \cdot y_{\frac{x_1}{\|x_1\|}} + x_2) + \mu = \lambda f(x) + \mu$. Finally, f is *normalization-equivariant*.

Proposition 2 (Operations preserving equivariance)

Proof: Let $x \in \mathbb{R}^n$, $\lambda \in \mathbb{R}_*^+$ and $\mu \in \mathbb{R}$.

- If f and g are both *scale-equivariant*, $(f \circ g)(\lambda x) = f(g(\lambda x)) = f(\lambda g(x)) = \lambda f(g(x)) = \lambda(f \circ g)(x)$ and if they are both *shift-equivariant*, $(f \circ g)(x + \mu) = f(g(x + \mu)) = f(g(x) + \mu) = f(g(x)) + \mu = (f \circ g)(x) + \mu$.
- Let $h : x \mapsto (f(x)^\top g(x)^\top)^\top$. If f and g are both *scale-equivariant*, $h(\lambda x) = (f(\lambda x)^\top g(\lambda x)^\top)^\top = (\lambda f(x)^\top \lambda g(x)^\top)^\top = \lambda h(x)$ and if they are both *shift-equivariant*, $h(x + \mu) = (f(x + \mu)^\top g(x + \mu)^\top)^\top = (f(x)^\top + \mu \quad g(x)^\top + \mu)^\top = h(x) + \mu$.
- Let $t \in \mathbb{R}$ and $h : x \mapsto (1-t)f + tg$. If f and g are both *scale-equivariant*, $h(\lambda x) = (1-t)f(\lambda x) + tg(\lambda x) = (1-t)\lambda f(x) + t\lambda g(x) = \lambda((1-t)f(x) + tg(x)) = \lambda h(x)$ and if they are both *shift-equivariant*, $h(x + \mu) = (1-t)f(x + \mu) + tg(x + \mu) = (1-t)(f(x) + \mu) + t(g(x) + \mu) = (1-t)f(x) + tg(x) + (1-t)\mu + t\mu = h(x) + \mu$.

Proposition 3

Proof: Let $a < b \in \mathbb{R}$, $f : \mathbb{R}^n \mapsto \mathbb{R}^m$, $x \in \mathbb{R}^n$, $\lambda \in \mathbb{R}_*^+$ and $\mu \in \mathbb{R}$.

We have $\mathcal{T}_{a,b}(\lambda x + \mu) = (b - a) \frac{\lambda x + \mu - \min(\lambda x + \mu)}{\max(\lambda x + \mu) - \min(\lambda x + \mu)} + a = (b - a) \frac{x - \min(x)}{\max(x) - \min(x)} + a = \mathcal{T}_{a,b}(x)$ ($\mathcal{T}_{a,b}$ is *normalization-invariant*). $\mathcal{T}_{a,b}^{-1}$ denotes the inverse transformation intricately linked to the input x of $\mathcal{T}_{a,b}$ (note that this is an improper notation as $\mathcal{T}_{a,b}$ is not bijective). Thus, if x is the input of $\mathcal{T}_{a,b}$, then $\mathcal{T}_{a,b}^{-1} : y \mapsto (\max(x) - \min(x)) \frac{y - a}{b - a} + \min(x)$.

$$\begin{aligned}
(\mathcal{T}_{a,b}^{-1} \circ f \circ \mathcal{T}_{a,b})(\lambda x + \mu) &= \frac{\max(\lambda x + \mu) - \min(\lambda x + \mu)}{b - a} ((f \circ \mathcal{T}_{a,b})(\lambda x + \mu) - a) + \min(\lambda x + \mu), \\
&= \lambda \frac{\max(x) - \min(x)}{b - a} ((f \circ \mathcal{T}_{a,b})(\lambda x + \mu) - a) + \lambda \min(x) + \mu, \\
&= \lambda \left(\frac{\max(x) - \min(x)}{b - a} ((f \circ \mathcal{T}_{a,b})(x) - a) + \min(x) \right) + \mu, \\
&= \lambda (\mathcal{T}_{a,b}^{-1} \circ f \circ \mathcal{T}_{a,b})(x) + \mu.
\end{aligned}$$

Finally, $\mathcal{T}_{a,b}^{-1} \circ f \circ \mathcal{T}_{a,b}$ is *normalization-equivariant*.

Proposition 4

Proof: f_θ^{NE} is composed of two types of building blocks of the following form:

- affine convolutions: $a_\Theta : x \in \mathbb{R}^n \mapsto \Theta x$ with $\Theta \in \mathbb{R}^{m \times n}$ subject to $\Theta \mathbf{1}_n = \mathbf{1}_m$,
- sort pooling nonlinearities: $\text{sortpool} : \mathbb{R}^n \mapsto \mathbb{R}^n$,

which are assembled using:

- function compositions: $\text{comp}(f, g) \mapsto f \circ g$,
- skip connections: $\text{skip}(f, g) \mapsto (x \mapsto (f(x)^\top g(x)^\top)^\top)$,
- affine residual connections: $\text{ares}_t(f, g) \mapsto (1-t)f + tg$ with $t \in \mathbb{R}$.

Note that the rows of Θ in a_Θ encode the convolution kernels in a CNN and the trainable parameters, denoted by θ , are only composed of matrices Θ and scalars t .

Since a_Θ and sortpool are *normalization-equivariant* functions, Prop. 2 states that the resulting function f_θ^{NE} is also *normalization-equivariant*. Moreover, since they are continuous and the assembling operators preserve continuity, f_θ^{NE} is continuous. Then, for a given input $x \in \mathbb{R}^n$, we have $(\text{sortpool} \circ a_\Theta)(x) = a_{\pi(\Theta)}(x) = \pi(\Theta)x$, where π an operator acting on matrix Θ by permuting its rows (note that the permutation π is both dependent on x and Θ). Therefore, applying a pattern “conv affine + sortpool” simply amounts locally to a linear transformation. Thus, as the nonlinearities of f_θ^{NE} are exclusively brought by sort pooling patterns, f_θ^{NE} is actually locally linear. In other words, f_θ^{NE} is piecewise-linear. Moreover, as there is a finite number (although high) of possible permutations of the rows of all matrices Θ , f_θ^{NE} has finitely many pieces. Finally, on each piece represented by the vector y_r , $f_\theta^{\text{NE}}(y) = A_\theta^{y_r} y$. It remains to prove that $A_\theta^{y_r} \mathbf{1}_n = \mathbf{1}_m$. But this property is easily obtained by noticing that, subject to dimensional compatibility on matrices Θ :

- $\Theta \mathbf{1}_n = \mathbf{1}_m \Rightarrow \pi(\Theta) \mathbf{1}_n = \mathbf{1}_m$ (“conv affine + sortpool”),
- $\Theta_1 \mathbf{1}_n = \mathbf{1}_m$ and $\Theta_2 \mathbf{1}_m = \mathbf{1}_l \Rightarrow \Theta_2 \Theta_1 \mathbf{1}_n = \mathbf{1}_l$ (composition),
- $\Theta_1 \mathbf{1}_{n_1} = \mathbf{1}_{m_1}$ and $\Theta_2 \mathbf{1}_{n_2} = \mathbf{1}_{m_2} \Rightarrow \begin{pmatrix} \Theta_1 \\ \Theta_2 \end{pmatrix} \mathbf{1}_{n_1+n_2} = \mathbf{1}_{m_1+m_2}$ (skip connection),
- $\Theta_1 \mathbf{1}_n = \mathbf{1}_m$ and $\Theta_2 \mathbf{1}_n = \mathbf{1}_m \Rightarrow (1-t)\Theta_1 \mathbf{1}_n + t\Theta_2 \mathbf{1}_n = \mathbf{1}_m$ (affine residual connection).

Thus, the affine combinations are preserved all along the layers of f_θ^{NE} . In the end,

$$f_\theta^{\text{NE}}(y) = A_\theta^{y_r} y, \text{ with } A_\theta^{y_r} \in \mathbb{R}^{m \times n} \text{ such that } A_\theta^{y_r} \mathbf{1}_n = \mathbf{1}_m.$$

D.2 Examples of normalization-equivariant conventional denoisers

Noise-reduction filters: All linear smoothing filters can be put under the form $f_\Theta : x \in \mathbb{R}^n \mapsto \Theta x$ with $\Theta \in \mathbb{R}^{n \times n}$ (the rows of Θ encode the convolution kernel). Obviously, f_Θ is always *scale-equivariant*, whatever the filter Θ . As for the *shift-equivariance*, a simple calculation shows that:

$$x \mapsto \Theta x \text{ is shift-equivariant} \Leftrightarrow \forall x \in \mathbb{R}^n, \forall \mu \in \mathbb{R}, \Theta(x + \mu \mathbf{1}_n) = \Theta x + \mu \mathbf{1}_m \Leftrightarrow \Theta \mathbf{1}_n = \mathbf{1}_m.$$

Since the sum of the coefficients of a Gaussian kernel and an averaging kernel is one, we have $\Theta \mathbf{1}_n = \mathbf{1}_m$, hence these linear filters are *normalization-equivariant*. The median filter is also *normalization-equivariant* because $\text{median}(\lambda x + \mu) = \lambda \text{median}(x) + \mu$ for $\lambda \in \mathbb{R}_*^+$ and $\mu \in \mathbb{R}$.

Patch-based denoising:

– NLM [20]: Assuming that the smoothing parameter h is proportional to σ , i.e. $h = \alpha\sigma$, we have $e^{-\frac{\|p(\lambda y_i + \mu) - p(\lambda y_j + \mu)\|_2^2}{(\alpha\lambda\sigma)^2}} = e^{-\frac{\lambda^2 \|p(y_i) - p(y_j)\|_2^2}{\lambda^2 (\alpha\sigma)^2}} = e^{-\frac{\|p(y_i) - p(y_j)\|_2^2}{h^2}}$, hence the aggregation weights are *normalization-invariant*. Then,

$$\begin{aligned} f_{\text{NLM}}(\lambda y + \mu, \lambda\sigma)_i &= \frac{1}{W_i} \sum_{y_j \in \Omega(y_i)} e^{-\frac{\|p(y_i) - p(y_j)\|_2^2}{h^2}} (\lambda y_j + \mu) \text{ with } W_i = \sum_{y_j \in \Omega(y_i)} e^{-\frac{\|p(y_i) - p(y_j)\|_2^2}{h^2}}, \\ &= \frac{1}{W_i} \sum_{y_j \in \Omega(y_i)} e^{-\frac{\|p(y_i) - p(y_j)\|_2^2}{h^2}} \lambda y_j + \frac{1}{W_i} \sum_{y_j \in \Omega(y_i)} e^{-\frac{\|p(y_i) - p(y_j)\|_2^2}{h^2}} \mu, \\ &= \lambda \left(\frac{1}{W_i} \sum_{y_j \in \Omega(y_i)} e^{-\frac{\|p(y_i) - p(y_j)\|_2^2}{h^2}} y_j \right) + \mu, \\ &= \lambda f_{\text{NLM}}(y, \sigma)_i + \mu. \end{aligned}$$

Finally, f_{NLM} is a *normalization-equivariant* function.

– NL-Ridge [27]: The block-matching procedure at the heart of NL-Ridge is *normalization-invariant* as it is based on comparisons of the ℓ_2 norm of the difference of image patches. For each noisy patch group, *a.k.a.* similarity matrix, $Y \in \mathbb{R}^{n \times k}$ composed of k vectorized similar patches of size n , the optimal weights $\Theta^* \in \mathbb{R}^{k \times k}$, in the ℓ_2 risk sense, are computed such that $Y\Theta^*$ is as close as possible to the (unknown) clean patch group $X \in \mathbb{R}^{n \times k}$. The two successive minimization problems approximating Θ under affine constraints $\mathcal{C} = \{\Theta \in \mathbb{R}^{k \times k}, \Theta^\top \mathbf{1}_k = \mathbf{1}_k\}$ can be put under the form:

$$\Theta^* = \arg \min_{\Theta \in \mathcal{C}} \text{tr} \left(\frac{1}{2} \Theta^\top Q \Theta + C \Theta \right) = I_k - n\sigma^2 \left[Q^{-1} - \frac{Q^{-1} \mathbf{1}_k (\mathbf{1}_k^\top Q^{-1})}{\mathbf{1}_k^\top Q^{-1} \mathbf{1}_k} \right].$$

with $Q = Y^\top Y$ or $Q = \hat{X}^\top \hat{X} + n\sigma^2 I_k$ for the first and second step, respectively (\hat{X} is the patch group estimate obtained after the first step), $C = n\sigma^2 I_k - Q$ and where tr denotes the trace operator. Depending on the step, we have:

$$2 \text{tr} \left(\frac{1}{2} \Theta^\top Q \Theta + C \Theta \right) = \begin{cases} \|Y\Theta - Y\|_F^2 + 2n\sigma^2 \text{tr}(\Theta) + \text{const} \\ \text{or} \\ \|\hat{X}\Theta - \hat{X}\|_F^2 + n\sigma^2 \|\Theta\|_F^2 + \text{const} \end{cases}$$

where $\|\cdot\|_F$ is the Frobenius norm. But, for any $Z \in \mathbb{R}^{n \times k}$ and any function $h : \Theta \in \mathbb{R}^{k \times k} \mapsto \mathbb{R}$,

$$\|(\lambda Z + \mu)\Theta - (\lambda Z + \mu)\|_F^2 + n(\lambda\sigma)^2 h(\Theta) = \lambda^2 (\|Z\Theta - Z\|_F^2 + n\sigma^2 h(\Theta)),$$

assuming that $\Theta^\top \mathbf{1}_k = \mathbf{1}_k$. Therefore, the aggregation weights Θ^* are *normalization-invariant* and $(\lambda Y + \mu)\Theta^* = \lambda Y\Theta^* + \mu$. Finally, NL-Ridge with affine constraints encodes a *normalization-equivariant* function.

TV denoising: Let $y \in \mathbb{R}^n$, $\lambda \in \mathbb{R}_*^+$ and $\mu \in \mathbb{R}$. Let $x^* = \arg \min_{x \in \mathbb{R}^n} \|x\|_{\text{TV}} \quad \text{s.t.} \quad \|y - x\|_2^2 = n\sigma^2$ be the solution of TV [18].

$$\begin{aligned}
f_{\text{TV}}(\lambda y + \mu, \lambda\sigma) &= \arg \min_{x \in \mathbb{R}^n} \|x\|_{\text{TV}} \quad \text{s.t.} \quad \|\lambda y + \mu - x\|_2^2 = n(\lambda\sigma)^2, \\
&= \arg \min_{x \in \mathbb{R}^n} \lambda \left\| \frac{x - \mu}{\lambda} \right\|_{\text{TV}} \quad \text{s.t.} \quad \lambda^2 \left\| y - \frac{x - \mu}{\lambda} \right\|_2^2 = \lambda^2 n\sigma^2, \\
&= \arg \min_{x \in \mathbb{R}^n} \left\| \frac{x - \mu}{\lambda} \right\|_{\text{TV}} \quad \text{s.t.} \quad \left\| y - \frac{x - \mu}{\lambda} \right\|_2^2 = n\sigma^2, \\
&= \lambda x^* + \mu, \\
&= \lambda f_{\text{TV}}(y, \sigma) + \mu.
\end{aligned}$$

Finally, f_{TV} is a *normalization-equivariant* function.